Spring 5-6-1952

The Study of An Unusual Augite Near Cabezon Peak, Sandoval County, New Mexico

George Brunton

THE STUDY OF AN UNUSUAL AUGITE NEAR CABEZON PEAK, SANDOVAL COUNTY, NEW MEXICO

By

George Brunton

A Thesis

In partial fulfillment of the

Requirements for the Degree of

Master of Science in Geology

The University of New Mexico

1952

This thesis, directed and approved by the candidate's committee, has been accepted by the Graduate Committee of the University of New Mexico in partial fulfillment of the requirements for the degree of

MASTER OF SCIENCE

E. A. Castetter

DEAN

5/6/52

DATE

Thesis committee

Carl W. Beck

CHAIRMAN

V. C. Kelley

J. Paul Fitzsimmons

CONTENTS

TABLES

PLATES

PLATE 1

Air View of Cabezon Peak

Nacimiento and Jemez Mountains in the background. Plug 5 is in the center foreground. Plugs 4 and 2 are in the left foreground and the left center, respectively.

(Photograph by courtesy of O. R. Lamsens and Dr. S. A. Wengerd)

PLATE 1

Air View of Cabezon Peak

Nacimiento and Jemez Mountains in the background. Plug 5 is in the center foreground. Plugs 4 and 2 are in the left foreground and the left center, respectively.

(Photograph by courtesy of O. R. Lampens and Dr. S. A. Wengerd)

PLATE 2

Sketch Map of Mount Taylor Volcanic Area

The plugs have been numbered for description starting with number 1, Cabezon Peak, in the upper right corner. Mount Taylor Mesa is now called Mesa Chivato.

Taken from D. W. Johnson, 1907, no scale given.

PLATE 2

Sketch Map of Mount Taylor Volcanic Area

The plugs have been numbered for description starting with number 1, Cabezon Peak, in the upper right corner. Mount Taylor Mesa is now called Mesa Chivato.

Taken from D. W. Johnson, 1907, no scale given.

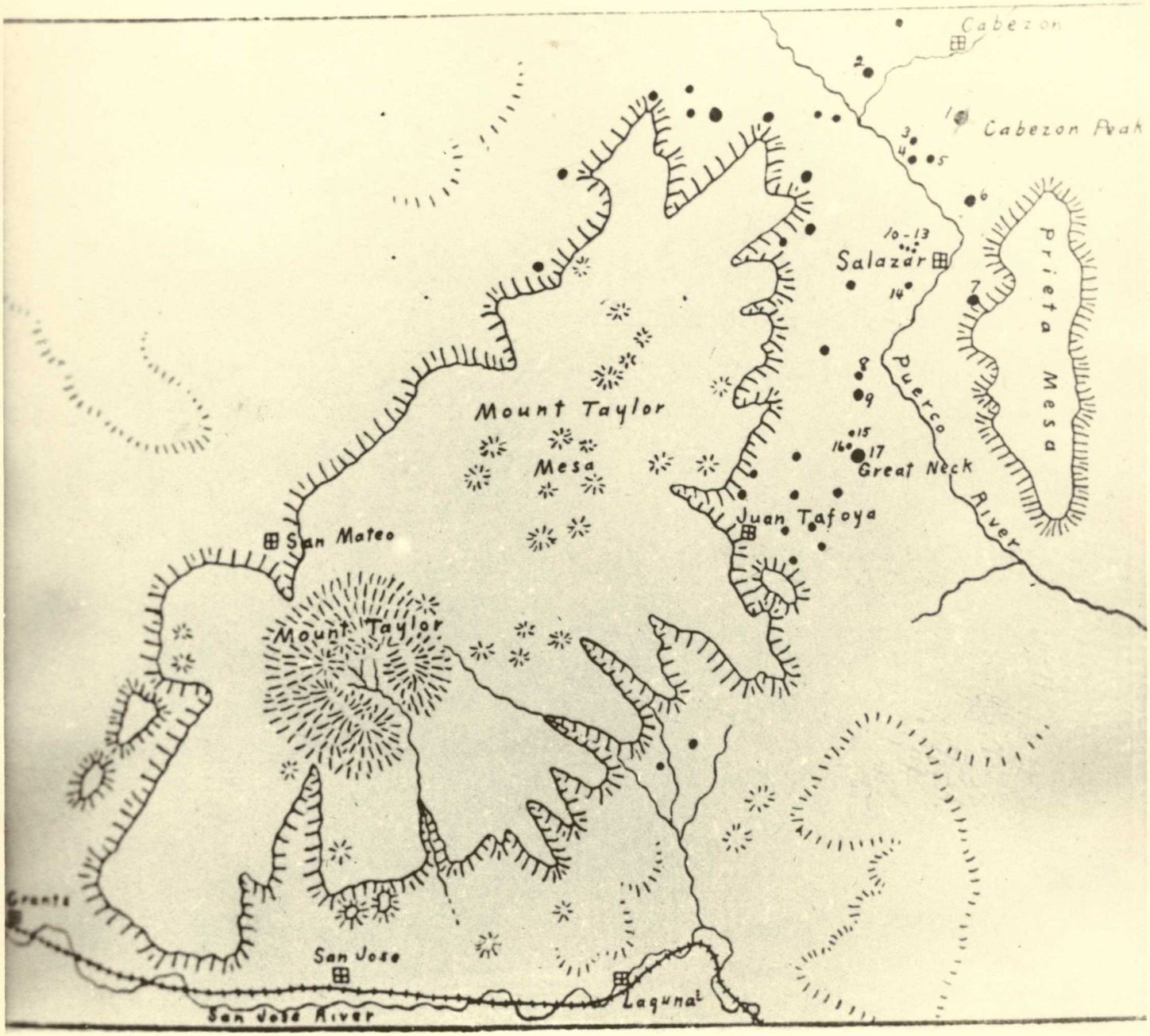
Cabezon
Cabezon Peak
Salazar
Prieta Mesa
Puerco
Great Neck
River
Mount Taylor
Mesa
Juan Tafoya
San Mateo
Mount Taylor
Grants
San Jose
Laguna
San Jose River

INTRODUCTION

When the writer was examining some of the volcanic plugs near Cabezon, New Mexico in the spring of 1951, he discovered in Plug No. 5 (Pl. 2, D. W. Johnson, 1907) some unusual, large vitreous inclusions. Plug 5 is about 70 miles northwest of Albuquerque, New Mexico and 5 miles southwest of Cabezon Peak, a prominent landmark in the southern San Juan Basin (Pl. 1). Plug 5 is in the northern part of T. 15 N., R. 4 W., New Mexico. It is accessible from Albuquerque via U. S. Highway 85 to Bernalillo, from Bernalillo west via State Highway 44 to a point about 15 miles north of San Ysidro and then westward about 20 miles on an unimproved dirt road through the settlement of Cabezon.

A brief study of the physical and chemical properties of the mineral inclusions failed to yield a positive identification, and therefore an x-ray powder photograph was made. The lines on the photograph were measured, and the d spacings of the three most intense lines were referred to the A. S. T. M. card file (A. S. T. M., 1950). The d spacings of the lines indicated that the mineral was probably a pyroxene, but they did not exactly coincide with any of the pyroxenes in the card file.

A quantitative chemical analysis by a graduate student of the Department of Chemistry at the University of New Mexico gave the following results:

Constituent	Percent
Fe_2O_3	2.07
FeO_3	10.98
BaO	1.09
CaO	20.63
NaO	6.42
SiO_2	49.59
Al_2O_3	7.14
OH	1.38
Total	99.30

When these percentages were transformed to molecular proportions and computed as a pyroxene, there was a discrepancy of half a molecule; consequently the mineral did not seem to be a pyroxene. The most interesting thing about the chemical analysis was the presence of BaO and the complete absence of MgO, the latter being present in nearly all natural pyroxenes.

Because of this evidence it was decided that the mineral was probably a new species. A complete x-ray examination by the rotation and Weissenberg single-crystal techniques was undertaken. As no small crystals of the mineral have been found, it was necessary to use tiny fragments and to orient them by x-ray methods. The tiny pieces have a cleavage which resembles a sub-conchoidal fracture, and what appears to be another very, very poor cleavage. The reflections from these cleavages are very poor and fuzzy; so that orientation of the fragment on the two-circle goniometer is impossible.

The first fragment was oriented with the axis of rotation normal to the cleavage that resembles a sub-

conchoidal fracture, and adjusted exactly parallel to a translation direction by a method to be described in the chapter on structural crystallography. A rotation photograph was taken and measured. The identity period of this translation direction is 6.61 A. Rotation pictures were taken about two other translation directions at right angles to the first and their lengths are 6.66 and 5.38 A. The lengths of the a, b, and c axes of augite are about 9.71, 8.89, and 5.24 (B. E. Warren and J. Biscoe, 1931, pp. 391).

Usually there are several translation directions in a monoclinic lattice, and in this particular one there are two extra, fortuitous directions perpendicular to the prismatic cleavages of the pyroxene and in the plane of the a and b axes. Two more rotation pictures were taken around axes parallel to the bisectors of the angles between the cleavages on the fragment. The lengths of these directions are 9.72 and 8.97 A. With the 5.38 A length of one of the first directions, these compare favorably with the unit cell dimensions of augite.

The x-ray evidence cast doubt upon the chemical analysis; therefore some of the original sample was fused with $KHSO_4$, dissolved in acid, the solution made strongly ammoniacal, and the solution tested for magnesium by the addition of dibasic sodium phosphate, Na_2HPO_4. An appreciable amount of NH_4MgPO_4 precipitated when the solution was allowed to stand overnight. Two more samples of the mineral were sent to the Department of Mineralogy and Petrography, Harvard

University, for quantitative chemical analyses. The results confirm the presence of MgO and indicate the mineral is a variety of augite.

Plug 5 and the other plugs of the Mount Taylor volcanic field are probably of late Miocene or Pliocene age (C. B. Hunt, 1937, p. 57).

ACKNOWLEDGMENTS

The writer wishes to acknowledge his indebtedness to Dr. Carl W. Beck who patiently guided the preliminary work and the writing of this paper; to Dr. V. C. Kelley and Dr. J. P. Fitzsimmons for their critical reading; to Charles Maxwell, A. L. Giorgi and others for their assistance in certain phases of the work.

PHYSICAL PROPERTIES

The specific gravity was determined on a Jolly balance by weighing the sample in air and then in water and applying the formula:

$$\text{Density (d)} = \frac{\text{Weight in air}}{\text{Weight in air- Weight in water}}$$

or

$$d = \frac{395}{395-281} = 3.46$$

The hardness, 5-6, and the cleavage, poor (110) at angles of 87° and 93°, are the same as those for other clinopyroxenes.

The luster is vitreous, almost resinous or pitchy in some specimens. The color is black in large pieces of the augite but yellowish green in thin slivers. Although the augite is almost opaque in large pieces, it is translucent on very thin edges.

No material showing crystal faces was found, but it is assumed that the morphological forms would be the same as in normal augite.

Some of the specimens show distinct front pinacoidal partings which are filled with fine calcite, clay, and iron oxide.

OPTICAL PROPERTIES

The optical properties of the augite were determined by matching the mineral with index liquids in sodium light.

$n_X = 1.695$ $n_Y = 1.699$ $n_Z = 1.713$

The optic plane is parallel to the {010} and the optic angle (2V) is 55°. The extinction angle ($X \wedge c$) is 45°. The optic sign is positive. The augite is not pleochroic.

STRUCTURAL CRYSTALLOGRAPHY

The structural crystallography was determined by a series of powder, rotation, and Weissenberg x-ray photographs.

The results of the powder photographs are shown in Table 1 where the d spacings of the Cabezon augite are compared to the d spacings of a specimen of augite from Bilin, Bohemia (A. S. T. M., 1950).

The d spacings or interplanar distances were computed from Braggs formula:

$$d = \frac{n \lambda}{2 \sin \theta}$$

4θ is the distance between two corresponding lines on a powder photograph and can be measured directly in millimeters. The distance is divided by four to give θ. λ is 1.9373 A for an iron target x-ray tube with a manganese

TABLE 1

The d Spacings of Two X-ray Powder Photographs of Augite

Plug 5		Bilin, Bohemia			
d A	I/I_1	d A	I/I_1	d A	I/I_1
7.19	4	3.31	5	1.51	6
4.63	1	3.26	5	1.49	5
4.46	3	3.20	6	1.46	2.5
3.58	3	2.99	10	1.45	2.5
3.33	4	2.94	7.5	1.43	10
3.21	6	2.86	6	1.41	8.5
2.99	10	2.77	5	1.39	5
2.92	6	2.56	8.5	1.38	5
2.89	6	2.51	8.5	1.33	8.5
2.56	5	2.36	2.5	1.28	8.5
2.53	3	2.29	5	1.27	5
2.50	5	2.20	5	1.25	7.5
2.29	3	2.13	7.5	1.22	2.5
2.21	2	2.04	7.5	1.19	2.5
2.13	5	2.00	6	1.18	2.5
2.10	2	1.97	5	1.15	5
2.03	5	1.93	2.5	1.14	2.5
2.00	3	1.82	7.5	1.09	5
1.82	2	1.78	2.5	1.08	10
1.75	4	1.74	7.5	1.07	10
1.67	3	1.71	2.5	1.07	10
1.63	1	1.68	6	1.06	5
1.62	4	1.66	6	1.05	2.5
1.61	1	1.62	10	1.04	6
1.55	.5	1.57	2.5	1.03	6
1.54	2	1.57	5	1.02	7.5
1.51	2	1.55	5	1.00	7.5
1.48	2	1.53	6		
1.41	6				
1.39	2				
1.33	1				
1.31	.5				
1.29	.5				
1.28	10				
1.25	.3				
1.24	.5				
1.15	3				
1.13	3				
1.07	1.5				
1.06	.5				
1.06	.3				

d	1/d
1.19	1
1.03	1
1.06	1
1.04	1
1.23	1
1.21	1
1.09	20
1.08	1
1.08	1
1.09	1
1.09	1
1.09	1
1.29	1
1.21	1
1.13	1
1.12	1
1.03	1
1.00	1
1.82	1
1.75	1
1.07	1
1.03	1
1.02	1
1.01	1
1.75	2
1.87	2
1.03	1
1.00	1
1.79	1
1.73	1
1.71	1
1.29	10
1.25	3
1.04	3
1.12	1
1.12	1
1.07	1
1.03	1
1.00	3

PLATE 3

Three X-ray Powder Photographs

The angle 2θ increases from top to bottom. Note the differences in the d spacings as 2θ becomes greater than 90° in the bottom halves of the photographs.

Figure 1. Augite from Plug 5.

Figure 2. Diopside from Hastings County, Ontario, Canada.

Figure 3. Augite -- Locality unknown.

PLATE 3

Three X-ray Powder Photographs

The angle 2θ increases from top to bottom. Note the differences in the d spacings as 2θ becomes greater than 90° in the bottom halves of the photographs.

Figure 1. Augite from Plug 5.

Figure 2. Diopside from Hastings County, Ontario, Canada.

Figure 3. Augite -- Locality unknown.

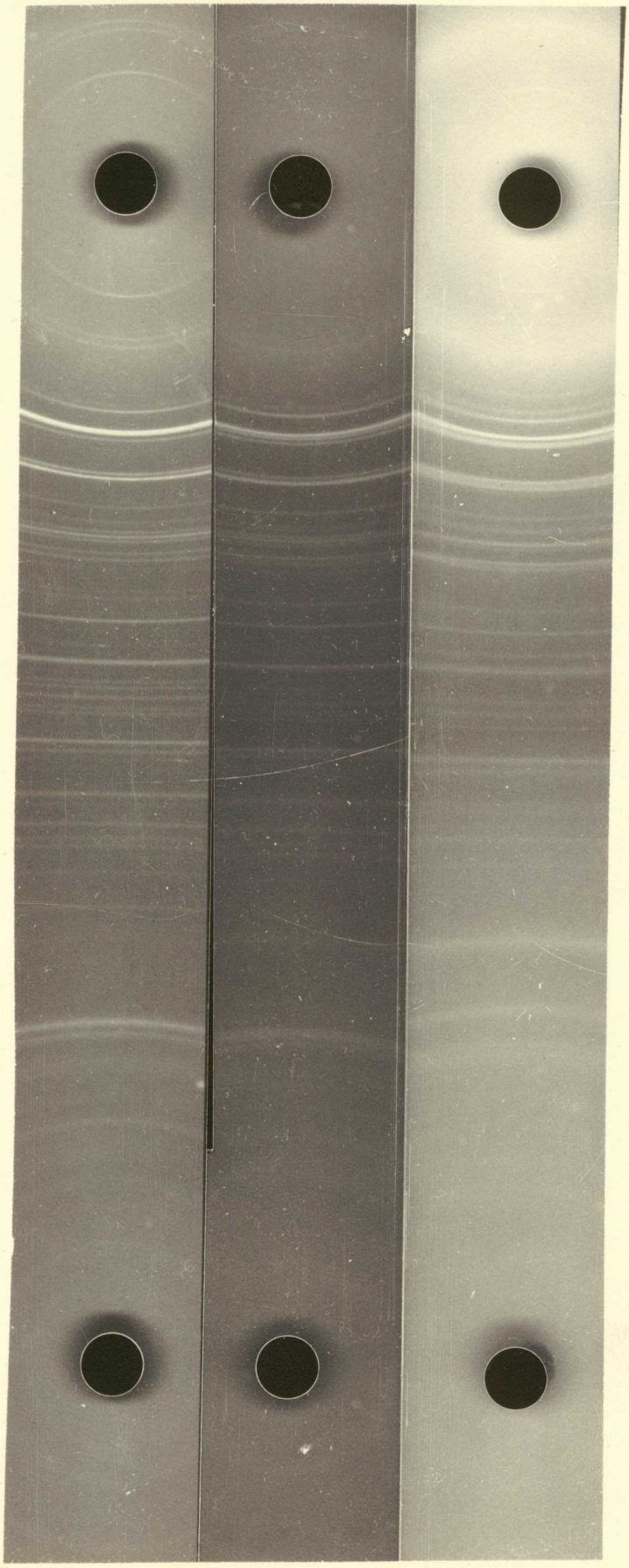
1
2
3

filter and n is a constant whose value is one.

The rotation and Weissenberg photographs were taken on a Weissenberg goniometer with an x-ray tube using an iron target and a manganese filter. The specimens were tiny fragments of the augite because no crystals were available. These fragments have a very poor cleavage which gives a poor reflection so that they cannot be oriented with the two-circle goniometer. It was necessary to orient the fragments by an x-ray method.

The x-ray method of adjusting a crystal fragment around a translation direction used by the writer is similar to that suggested by Bunn (1946) and the Donnays (1951, Preprint) but it differs in being simple and having no complicated formulae.

A fragment or poorly developed crystal of a mineral is mounted on the universal head of the two-circle goniometer in the usual manner. If there are any cleavages or other morphological features that may help in the orientation of the specimen, the mineral should be put on the goniometer and oriented in the same manner as the orientation of a perfectly formed crystal with the object of bringing some crystallographic axis as nearly as possible parallel to the axis of rotation.

The universal head is mounted on the Weissenberg with the large (L) circular arc on the head parallel to the x-ray beam and the small (S) circular arc normal

to the beam. The Weissenberg goniometer in the University of New Mexico Geology Department is in this position when it reads 279.2° on the vernier scale around the axis of rotation. The mechanism is then adjusted to oscillate 10° about this zero point--274° to 284°.

The Weissenberg camera is loaded with a strip of film 1¼ by 6½ inches in such a way that the long direction of the film is around the circumference of the camera and centered. One corner of the film is notched and this notch is placed in the upper right hand position in the camera as seen by the operator looking parallel to the direction of the x-ray beam. When the camera is in place before the x-ray beam, the specimen is oscillated 10° about the Weissenberg zero in an unfiltered x-ray beam for 10-30 minutes, then the proper filter is placed in the beam and the specimen is allowed to rotate 360° for a similar length of time. At no time is the film or camera moved.

The film is developed in the usual manner. It will have upon it the usual spot reflections and streaks radiating from the center direct beam spot (Pl. 5). These streaks are used to adjust the specimen more nearly parallel to the axis of rotation. If a translation direction of the crystal is parallel to the axis of rotation then the longest well-defined streak is a straight line parallel to the 0 layer line and perpendicular to the shadow of the direct beam absorbing target. If the crystal is not in adjustment

there will be a curved streak that will make some angle less than 20° with an imaginary straight line where the 0 layer line should be. The amount and direction of curvature of this streak depends upon the angle and direction of displacement of the translation axis with respect to the axis of rotation in the planes of the S and L arcs of the universal head (Bunn, 1946, pp. 173).

If the translation axis is displaced only in the plane of the S arc, the streak forms an arc that is symmetrically disposed on either side of the imaginary 0 layer line with its maximum curvature at 1/4 and 3/4 of the length of the film and its minimum at the center and ends (Pl. 4, fig. 1). Because the plane of the displacement parallels the plane of the film, it is possible to measure the amount of deviation directly from the film by means of a protractor. The angle of deviation will be the angle between the streak and the imaginary 0 layer line in the center of the film--the angle ϕ in Pl. 4, fig. 1.

Fig. 2 shows an example of deviation of $\phi°$, the method of measurement and a view of the S arc showing the direction of correction.

If the deviation of the translation axis is in the plane of the L arc, the streak will resemble Pl. 4, fig. 3 with the streaks on both halves of the film on the same side of the imaginary 0 layer line and with their maxima at the ends of the film and minima in the center. The plane

of the L arc is perpendicular to the plane of the film at the direct beam spot and so is the plane of the reciprocal lattice which rotates in the direct beam spot; thus from a top view of the camera it is apparent that for small angles of deviation θ, x in millimeters equals θ in degrees.

Pl. 4, fig. 4 shows derivation of the formula and shows the necessary correction on the L arc.

For a combination of deviations in both the S and L arcs the streak appears approximately as in Pl. 4, fig. 5 and it is necessary to measure both ϕ and x, or θ, and correct for each.

This method leads only to approximate adjustments and it takes some experience and 3 to 5 photographs per orientation to line up the axis of translation exactly parallel to the axis of rotation. The most difficult part of the orientation is when the angles of deviation are very small. Sometimes it is necessary to look at the first and second layer lines to be sure of the direction of deviation and the arc affected. The first and second layer lines do not have streaks but, when the angles become very small, the deviation is apparent in these lines because of natural exaggeration; therefore, the direction is easy to see even in angles of less than half a degree.

Pl. 5 shows three photographs used to orient a specimen and shows various misadjustments. Fig. 3, Pl. 5 is an adjusted photograph.

PLATE 4

Five Figures to be used with the
Orientation of Crystal Fragments
by X-ray Methods

Figure 1. A deviation of ϕ on the small arc, S.

Figure 2. The method of measuring ϕ and the direction of adjustment on the small arc.

Figure 3. The deviation $\underline{x}$ on the large arc, L.

Figure 4. The derivation of the angle θ from the measured length $\underline{x}$ and the direction of correction to be applied to the large arc.

Figure 5. The result of deviations in both arcs at the same time.

PLATE 4

Five Figures to be used with the Orientation of Crystal Fragments by X-ray Methods

Figure 1. A deviation of ϕ on the small arc, S.

Figure 2. The method of measuring ϕ and the direction of adjustment on the small arc.

Figure 3. The deviation x on the large arc, L.

Figure 4. The derivation of the angle θ from the measured length x and the direction of correction to be applied to the large arc.

Figure 5. The result of deviations in both arcs at the same time.

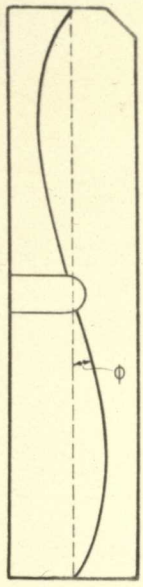

FIGURE 1

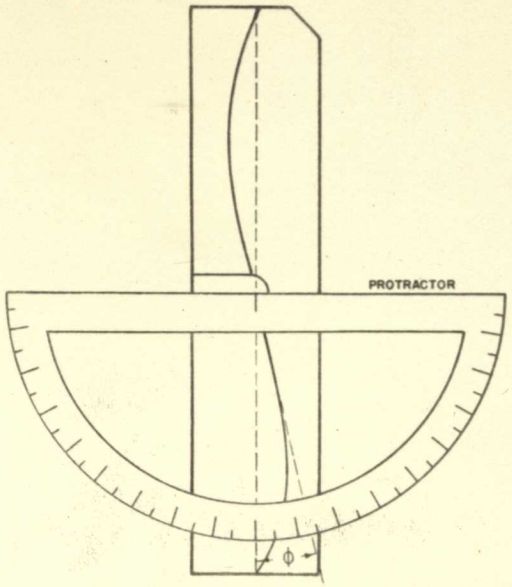

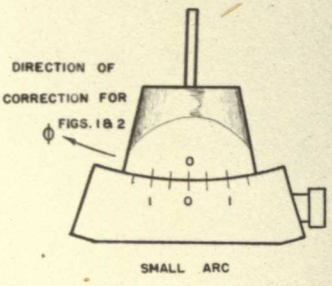

FIGURE 2

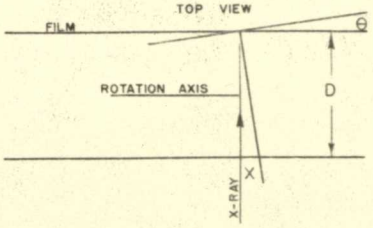

θ = ANGLE OF TILT

D = DIAM. OF CAMERA

X = θD IN RADIANS

OR

X = θ IN MM , IF D = 57.3 MM

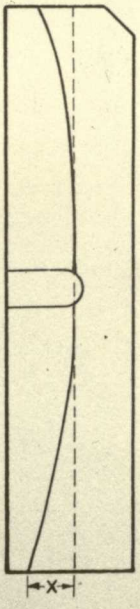

FIGURE 3

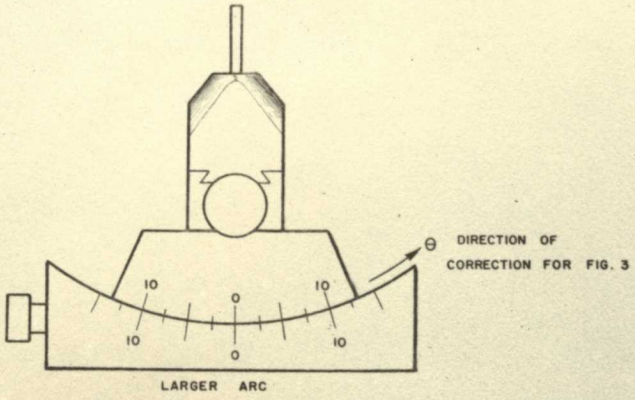

FIGURE 4

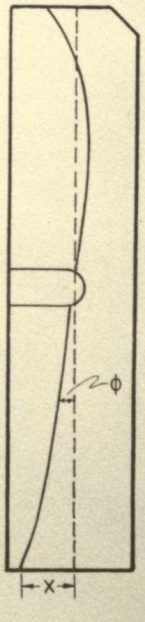

FIGURE 5

After the augite fragments were adjusted, rotation photographs were taken. Pl. 6, fig. 4 shows the first rotation picture which has an identity period of 6.61 A. Pl. 7, fig. 1 is one of several symmetry photographs taken around this axis to determine the symmetry of the crystal. All the photographs were similar to fig. 1 which has no symmetry. If the mineral were monoclinic prismatic, there would have been either two showing a plane of symmetry or one with a plane of symmetry and the other with a two-fold axis when the x-ray beam was parallel to each of the other two crystallographic axes. Therefore, the mineral seemed to be triclinic.

It is not good practice to rely upon just one rotation to establish the symmetry and unit cell dimensions of a mineral, particularly in the low symmetry classes, because of the possibility of more than three translation directions. It is necessary to pick a number of these directions to establish the maximum symmetry of the crystal and then to choose as crystallographic axes the three identity periods that define the smallest unit cell.

A rotation was made about an axis parallel to the cleavage (Pl. 6, fig. 3) and the identity period was 5.38 A. Two symmetry photographs were taken parallel to the translations chosen as the other two probable axes from a Weissenberg 0 layer line photograph (Pl. 7, figs. 3 and 4). They show a plane of symmetry and a two-fold axis of sym-

PLATE 5

Three Adjustment X-ray Photographs

(natural size)

Figure 1. The adjustment should be, right 5°, small arc and left 4°, large arc.

Figure 2. The adjustment should be, left 1°, small arc and right 2°, large arc.

Figure 3. Perfect adjustment.

PLATE 5

Three Adjustment X-ray Photographs

(natural size)

Figure 1. The adjustment should be, right 5°, small arc and left 4°, large arc.

Figure 2. The adjustment should be, left 1°, small arc and right 2°, large arc.

Figure 3. Perfect adjustment.

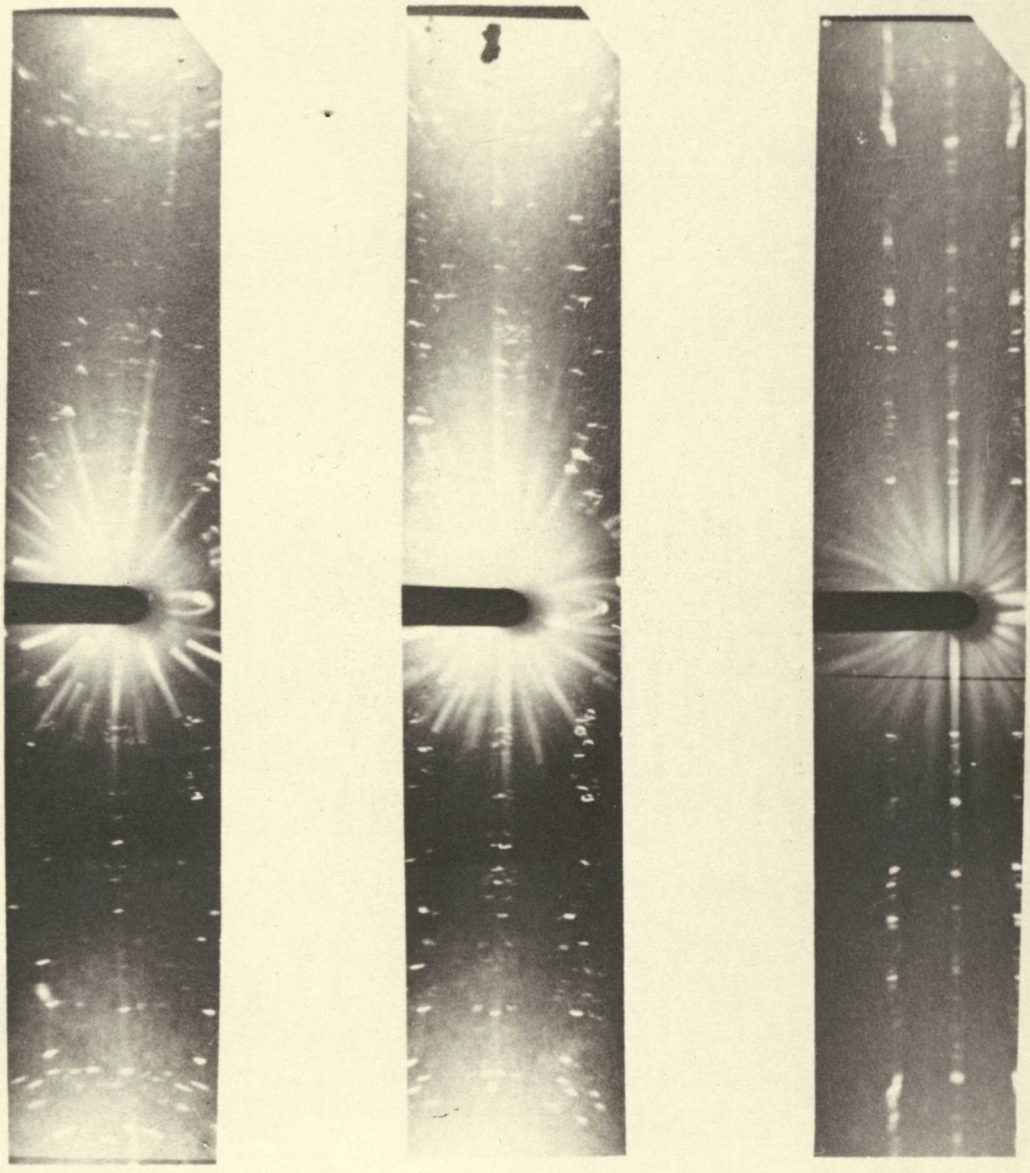

1 2 3

metry respectively. Additional rotations were made about these two translations (Pl. 6, figs. 1 and 2) and the identity periods are 9.54 and 8.92 A respectively (Table 2). The identity periods were calculated from the formula:

$$t = \frac{n\lambda}{\sin \tan^{-1} y/r}$$

where λ is the wave length of the x radiation, in this case iron $K\alpha$ which is 1.9373 A; n is the number of the layer line; y the distance from the 0 layer line to the n layer line; and r the radius of the Weissenberg camera, 28.65 mm.

Another symmetry photograph was taken parallel to the 5.38 A axis and it showed a plane of symmetry (Pl. 7, fig. 2); therefore, the crystal has a monoclinic prismatic symmetry, a plane and a two-fold axis.

The observed Weissenberg diffractions conform to the following conditions: (hkl) present when $h + k = 2n$, (h0l) present when $h = 2n$ and $l = 2n$, and (0k0) present when $k = 2n$; these criteria are characteristic for the space group C_{2c} (Internationale Tabellen, 1944). This space group is the same as that for augite. The unit cell dimensions for augite, a = 9.71, b = 8.89 and c = 5.24 (B. E. Warren and J. Biscoe, 1931, pp. 391) and the cell dimensions in Table 2 are very nearly the same. The differences are probably due to the slight changes in chemical composition which would expand or contract the lattice to accommodate changes in ionic radii; for example, substitution of aluminum for silicon should expand the lattice along the c

axis proportional to the amount of substitution.

The monoclinic angle β may be calculated from b-axis rotation Weissenberg 0 layer line by the formula:

$$\beta = 2w \text{ or } \beta = 180^\circ - 2w$$

depending upon the orientation of the crystal in the camera. The measured values of w averaged 52.045 mm. β in this case equals $2w$ or $104^\circ 5'$.

TABLE 2

Computation of the Identity Period from Rotation Photographs

Rotation around a axis

$$t_1 = \frac{1 \times 1.9373}{\sin \tan^{-1}(5.78/28.65)} = 9.59 \text{ A}$$

$$t_2 = \frac{2 \times 1.9373}{\sin \tan^{-1}(12.41/28.65)} = 9.75 \text{ A}$$

$$t_3 = \frac{3 \times 1.9373}{\sin \tan^{-1}(21.05/28.65)} = 9.82 \text{ A}$$

$$t_4 = \frac{4 \times 1.9373}{\sin \tan^{-1}(37.73/28.65)} = 9.73 \text{ A}$$

9.54 A is the a lattice dimension measured from powder photograph

Rotation around b axis

$$t_1 = \frac{1 \times 1.9373}{\sin \tan^{-1}(6.35/28.65)} = 8.95 \text{ A}$$

$$t_2 = \frac{2 \times 1.9373}{\sin \tan^{-1}(13.68/28.65)} = 8.99 \text{ A}$$

$$t_3 = \frac{3 \times 1.9373}{\sin \tan^{-1}(24.40/28.65)} = 8.96 \text{ A}$$

8.92 A is the b lattice dimension measured from powder photograph

Rotation around c axis

$$t_1 = \frac{1 \times 1.9373}{\sin \tan^{-1}(11.08/28.65)} = 5.37 \text{ A}$$

$$t_2 = \frac{2 \times 1.9373}{\sin \tan^{-1}(29.60/28.65)} = 5.39 \text{ A}$$

5.30 A is the c lattice dimension measured from powder photograph

$$\theta_1 = \frac{1 \times 1.9173}{\sin \tan^{-1}(\quad)} =$$

$$\theta_2 = \frac{2 \times 1.9173}{\sin \tan^{-1}(\quad)} =$$

$$\theta_3 = \frac{1 \times 1.9173}{\sin \tan^{-1}(\quad)} =$$

$$\theta_4 = \frac{4 \times 1.9173}{\sin \tan^{-1}(\quad)} =$$

$$\theta_1 = \frac{1 \times 1.9173}{\sin \tan^{-1}(\quad)} =$$

$$\theta_2 = \frac{2 \times 1.9173}{\sin \tan^{-1}(\quad)} =$$

$$\theta_3 = \frac{3 \times 1.9173}{\sin \tan^{-1}(\quad)} =$$

$$\theta_1 = \frac{1 \times 1.9173}{\sin \tan^{-1}(\quad)} =$$

$$\theta_2 = \frac{2 \times 1.9173}{\sin \tan^{-1}(\quad)} =$$

PLATE 6

Four X-ray Rotation Photographs

(2/3 natural size)

Figure 1. The a axis rotation.

Figure 2. The b axis rotation.

Figure 3. The c axis rotation.

Figure 4. Rotation perpendicular to the {110}.

PLATE 6

Four X-ray Rotation Photographs

(2/3 natural size)

Figure 1. The a axis rotation.

Figure 2. The b axis rotation.

Figure 3. The c axis rotation.

Figure 4. Rotation perpendicular to the {110}.

FIGURE 1

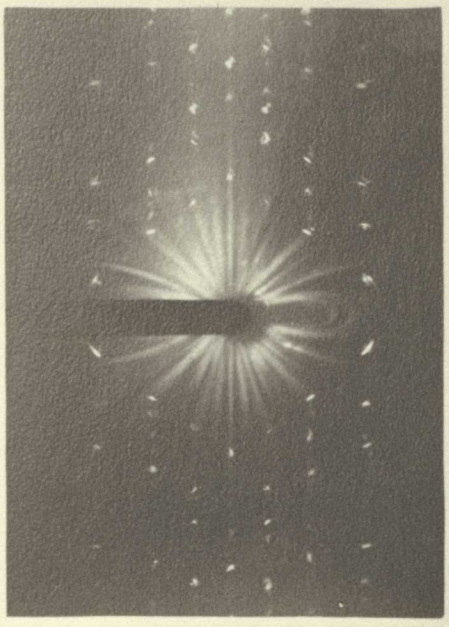

FIGURE 2

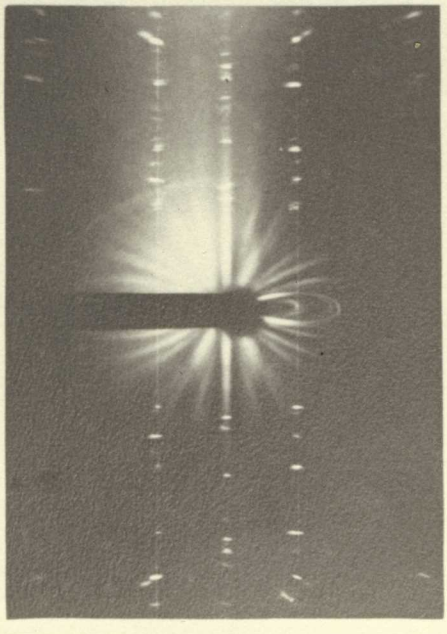

FIGURE 3

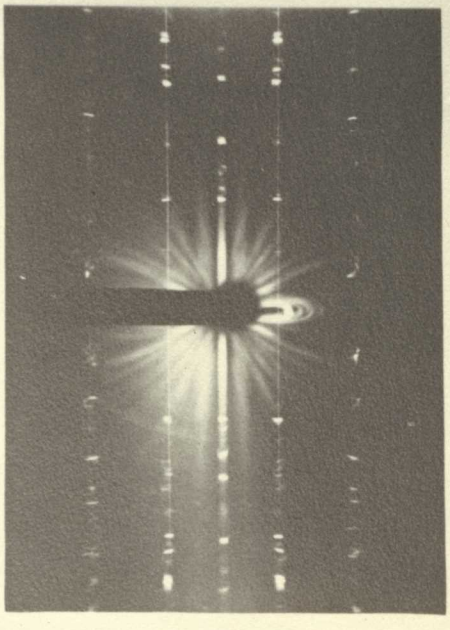

FIGURE 4

PLATE 7

Four X-ray Symmetry Photographs

(2/3 natural size)

Figure 1. No symmetry.

Figure 2. Plane of symmetry.

Figure 3. Plane of symmetry.

Figure 4. Two-fold axis of symmetry.

PLATE 7

Four X-ray Symmetry Photographs

(2/3 natural size)

Figure 1. No symmetry.

Figure 2. Plane of symmetry.

Figure 3. Plane of symmetry.

Figure 4. Two-fold axis of symmetry.

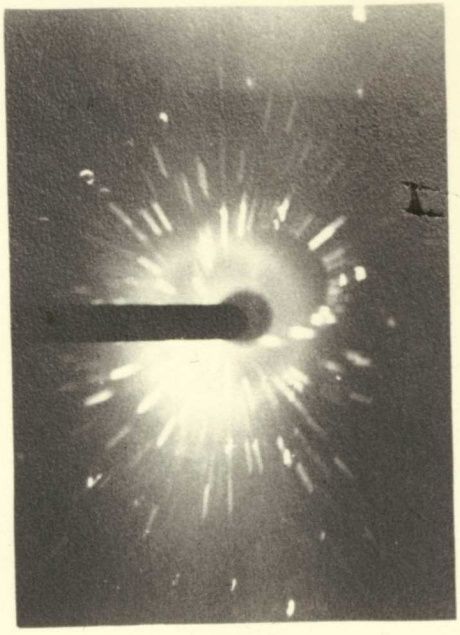

FIGURE 1

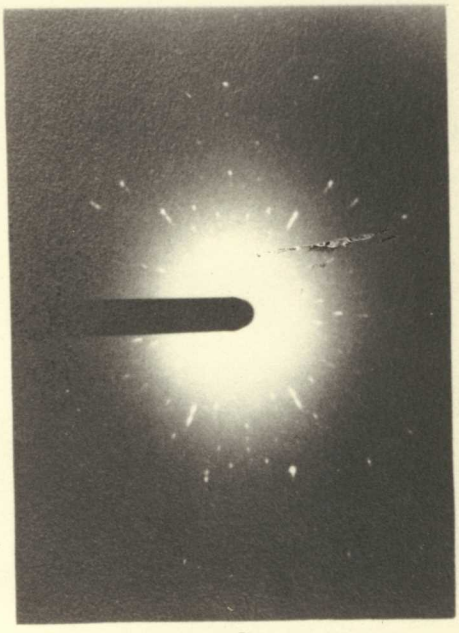

FIGURE 2

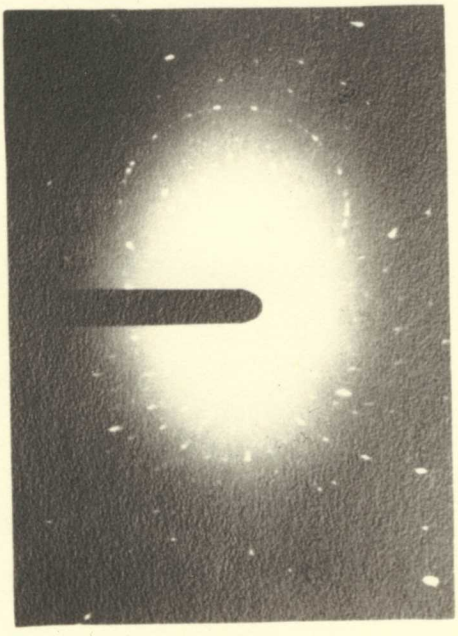

FIGURE 3

FIGURE 4

CHEMICAL COMPOSITION AND CELL CONTENT

Two chemical analyses were made of the Cabezon augite, F. A. Gonyer, analyst, and the results are as follows:

Sample 1.

Constituent	Percent
SiO_2	48.8
Al_2O_3	7.1
TiO_2	0.2
FeO	8.9
MgO	17.6
CaO	16.2
Na_2O	1.2
Total	100.0

Sample 2.

SiO_2	48.56
Al_2O_3	9.86
TiO_2	1.29
Fe_2O_3	2.36
FeO	6.22
MnO	0.09
MgO	14.44
CaO	15.88
Na_2O	1.16
K_2O	0.04
H_2O^+	0.02
H_2O^-	0.06
Total	99.83

Calculation of the empirical formulas as shown in Tables 3 and 4 yield the following:

Sample 1. $(Ca_{.64},Mg_{.28},Na_{.04})(Mg_{.79},Fe_{.28})(Si_{.80},Al_{.15})SiO_6$ or $(Ca,Mg,Na)_{.96}(Mg,Fe)_{1.05}(Si,Al)_{.95}SiO_6$

Sample 2. $(Ca_{.62},Mg_{.17},Na_{.04})(Mg_{.62},Fe^{++}_{.19},Fe^{+++}_{.03})(Si_{.78},Al_{.21},Ti_{.03})SiO_6$

or $(Ca,Mg,Na)_{.83}(Mg,Fe^{++},Fe^{+++})_{.84}(Si,Al,Ti)_{1.02}SiO_6$

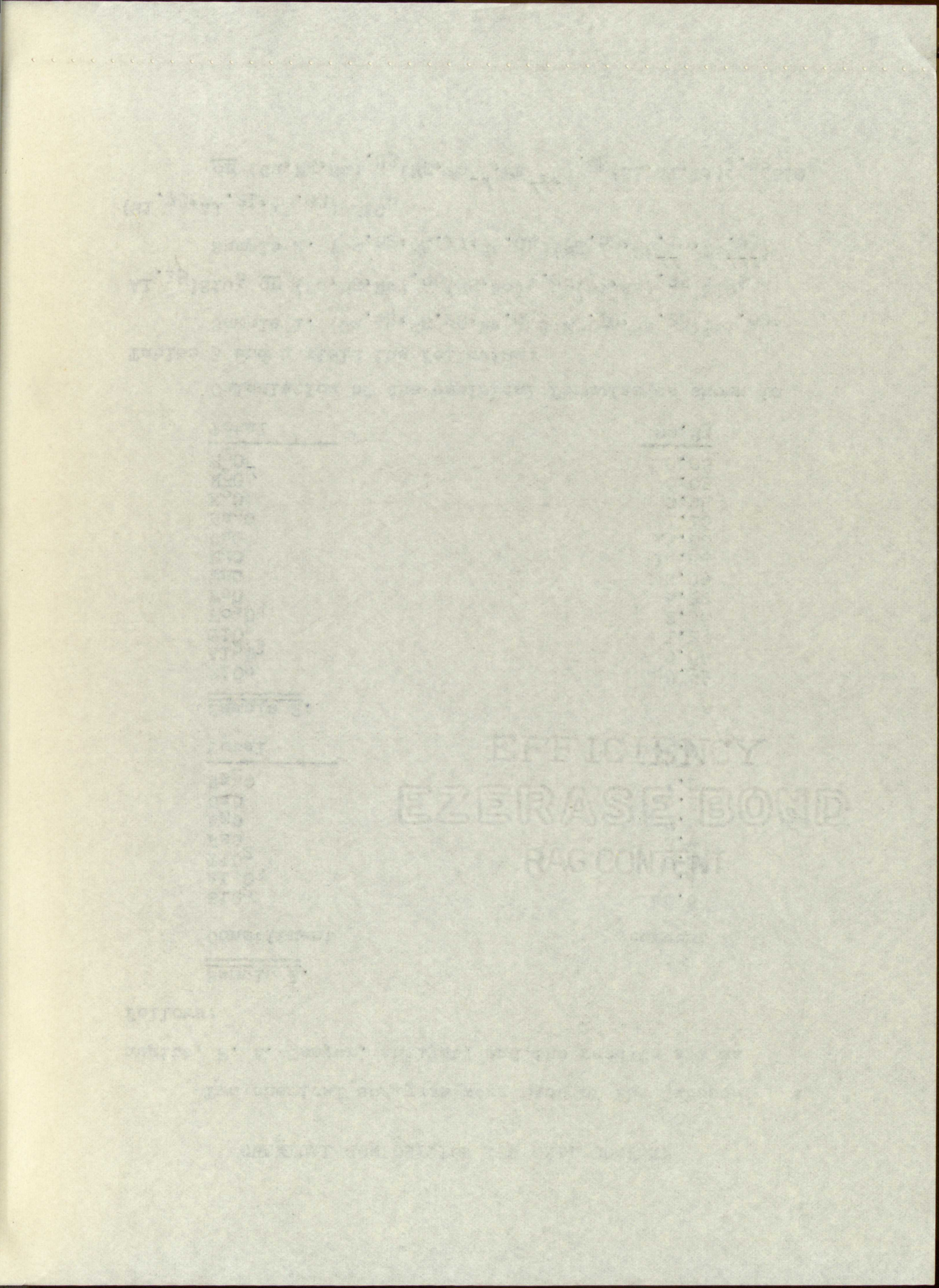
EFFICIENCY
EZERASE BOND
RAG CONTENT

TABLE 3

Determination of the Empirical Formula, Sample 1

	Molecular Proportion	Molecular Ratio
$\frac{\text{Percent } SiO_2}{\text{Mol. wt.} SiO_2} = \frac{48.8}{60.06}$	1.63	1.80
$\frac{\text{Percent } Al_2O_3}{\text{Mol. wt.} Al_2O_3} = \frac{7.1}{101.94}$	.21	.15
$\frac{\text{Percent } TiO_2}{\text{Mol. wt.} TiO_2} = \frac{0.2}{79.90}$	.01	.01
$\frac{\text{Percent FeO}}{\text{Mol. wt.FeO}} = \frac{8.9}{71.84}$	.13	.28
$\frac{\text{Percent MgO}}{\text{Mol. wt.MgO}} = \frac{17.6}{40.32}$	.44	.97
$\frac{\text{Percent CaO}}{\text{Mol. wt.CaO}} = \frac{16.2}{56.08}$	.29	.64
$\frac{\text{Percent } Na_2O}{\text{Mol. wt.} Na_2O} = \frac{1.2}{61.99}$	.02	.04
	Total: 2.73	

The molecular ratio is determined by the formula

$$\text{Molecular ratio} = \frac{\text{Molecular proportion}}{6/\text{Total of molecular proportions}}$$

where 6 is the number of oxygen atoms in a clinopyroxene molecule.

TABLE 4

Determination of the Empirical Formula, Sample 2

	Molecular Proportion	Molecular Ratio
$\frac{\text{Percent } SiO_2}{\text{Mol. wt.} SiO_2} = \frac{48.56}{60.06}$	1.62	1.78
$\frac{\text{Percent } Al_2O_3}{\text{Mol. wt.} Al_2O_3} = \frac{9.86}{101.94}$	.29	.21
$\frac{\text{Percent } TiO_2}{\text{Mol. wt.} TiO_2} = \frac{1.29}{79.90}$	.03	.04
$\frac{\text{Percent FeO}}{\text{Mol. wt.FeO}} = \frac{6.22}{71.84}$	.09	.19
$\frac{\text{Percent } Fe_2O_3}{\text{Mol. wt.} Fe_2O_3} = \frac{2.36}{159.68}$	.04	.03
$\frac{\text{Percent MgO}}{\text{Mol. wt.MgO}} = \frac{14.44}{40.32}$	.36	.79
$\frac{\text{Percent CaO}}{\text{Mol. wt.CaO}} = \frac{15.88}{56.08}$	.28	.62
$\frac{\text{Percent } Na_2O}{\text{Mol. wt.} Na_2O} = \frac{1.39}{61.99}$	.02	.05
	Total: 2.73	

The percentages of the other elements reported are so small that they may be ignored in the calculation of the empirical formula.

The structural lattice dimensions combined with the measured specific gravity (3.46) and the chemical analysis of the material gives the number of molecules in the unit cell:

$$\text{density} = \frac{\text{weight}}{\text{volume}}$$

$$d = \frac{nM \times 1.649 \times 10^{-24}}{a \times b \times c \times \sin\beta}$$

where M = mass of the chemical unit of which the crystal is composed, d = density, a x b x c x sin β = volume of the unit cell, and n = number of molecules in the unit cell. 1.649×10^{-24} is Avogadro's number which changes units of atomic weight into grams.

$$3.46 = \frac{n \times 216.7 \times 1.649 \times 10^{-24}}{9.54 \times 8.92 \times 5.30 \times \sin 104^{\circ}\ 5'}$$

When this equation is solved for n, n equals 4.05 or approximately 4. When 4 is substituted into the formula and solved for d using the molecular weights of samples 1 and 2, d equals 3.27 and 3.19.

PLATE 8

Plug 5 from the South

The prominent dike in the foreground is the major source of the augite phenocrysts.

PLATE 8

Plug 5 from the South

The prominent dike in the foreground is the major source of the augite phenocrysts.

PETROGRAPHY AND PETROLOGY

Macroscopic

The rock in Plug 5 is a porphyritic olivine basalt with large granular inclusions of olivine and/or diopside and enstatite. The inclusions are not individual crystals but aggregates of a great number of small crystals about ½ to 1 mm. in diameter. The inclusions are probably cumular-sphäroliths and the rock would be cumulophyric (Johannsen, 1939, Vol. 1, pp. 172 and 207). The cumulars phäroliths range from slightly less than ½ inch to 6 inches (Pl. 10 and Pl. 11, fig. 1). Some of the cumulars phäroliths are composed entirely of yellow olivine but more commonly they are a mixture of olivine, diopside, enstatite, and spinel. Some of them are composed entirely of diopside, enstatite, and spinel in the ratio of about 10:5:1 respectively. All these minerals are, in general, equigranular.

There are unusual phenocrysts of augite that vary in size from 1/8 inch to 3 inches. None of the phenocrysts shows any crystal outlines but are commonly rounded or elliptical. They resemble xenoliths rather than phenocrysts. The majority of the augite crystals are dark gray, lusterless, and impure, containing grains of enstatite and commonly calcite as an alteration product. Some of the augite is very pure and looks like obsidian.

Sandstone xenoliths are common in the dike to the south of the plug and in the plug itself. The augite occurs near the sandstone xenoliths. Some of the sandstone blocks are as much as 1 to 2 feet in diameter. Most of the sandstone seems to be derived from the Mesaverde formation which is the predominant surface rock. Plug 5 and the other plugs have intruded the flat-lying Mesaverde sandstone and shale of late Cretaceous age and seem to have accumulated the xenoliths by plucking them from the walls during intrusion (Pls. 1 and 8).

Aragonite and calcite fill or partly fill voids in the basalt and are probably alteration products derived from the weathering of the feldspars in the rock.

Microscopic

The rock is a porphyritic olivine basalt. The feldspar is labradorite, An_{50}, and comprises 70 percent of the rock. It occurs principally as microlites nearly always twinned once according to the albite law. There are a few anhedral phenocrysts of labradorite that show polysynthetic albite twinning (Pl. 12, fig. 1). The microlite laths give the rock a felty appearance and occasionally show flow structure.

Olivine occurs as small 40 to 1000 μ phenocrysts distributed throughout the groundmass and as cumularsphäroliths. The larger crystals often have a dark reaction rim

PLATE 9

Augite Phenocryst in Basalt Dike

The black phenocryst to the left and slightly above the pencil point is augite. It occurs in the dike shown in Plate 8.

PLATE 9

Augite Phenocryst in Basalt Dike

The black phenocryst to the left and slightly above the pencil point is augite. It occurs in the dike shown in Plate 6.

PLATE 10

Cumulariphärolith in Basalt Dike

The cumulariphärolith near the pencil eraser is composed of diopside, enstatite, and olivine. Above the pencil are an augite crystal and another smaller cumulariphärolith. This picture was taken near the site of Plate 9.

PLATE 10

Cumularsphärolith in Basalt Dike

The cumularsphärolith near the pencil eraser is composed of diopside, enstatite, and olivine. Above the pencil are an augite crystal and another smaller cumular-sphärolith. This picture was taken near the site of Plate 9.

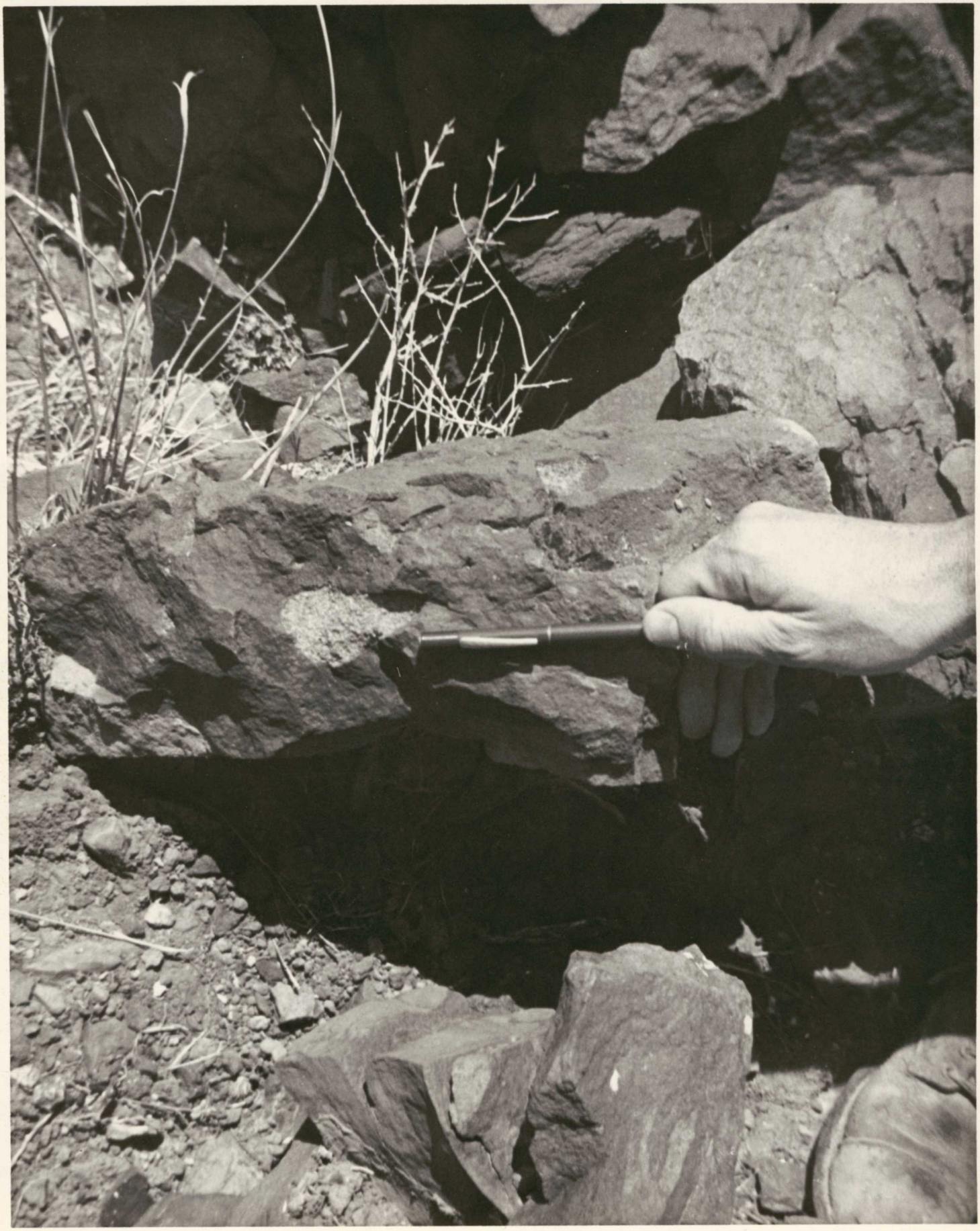

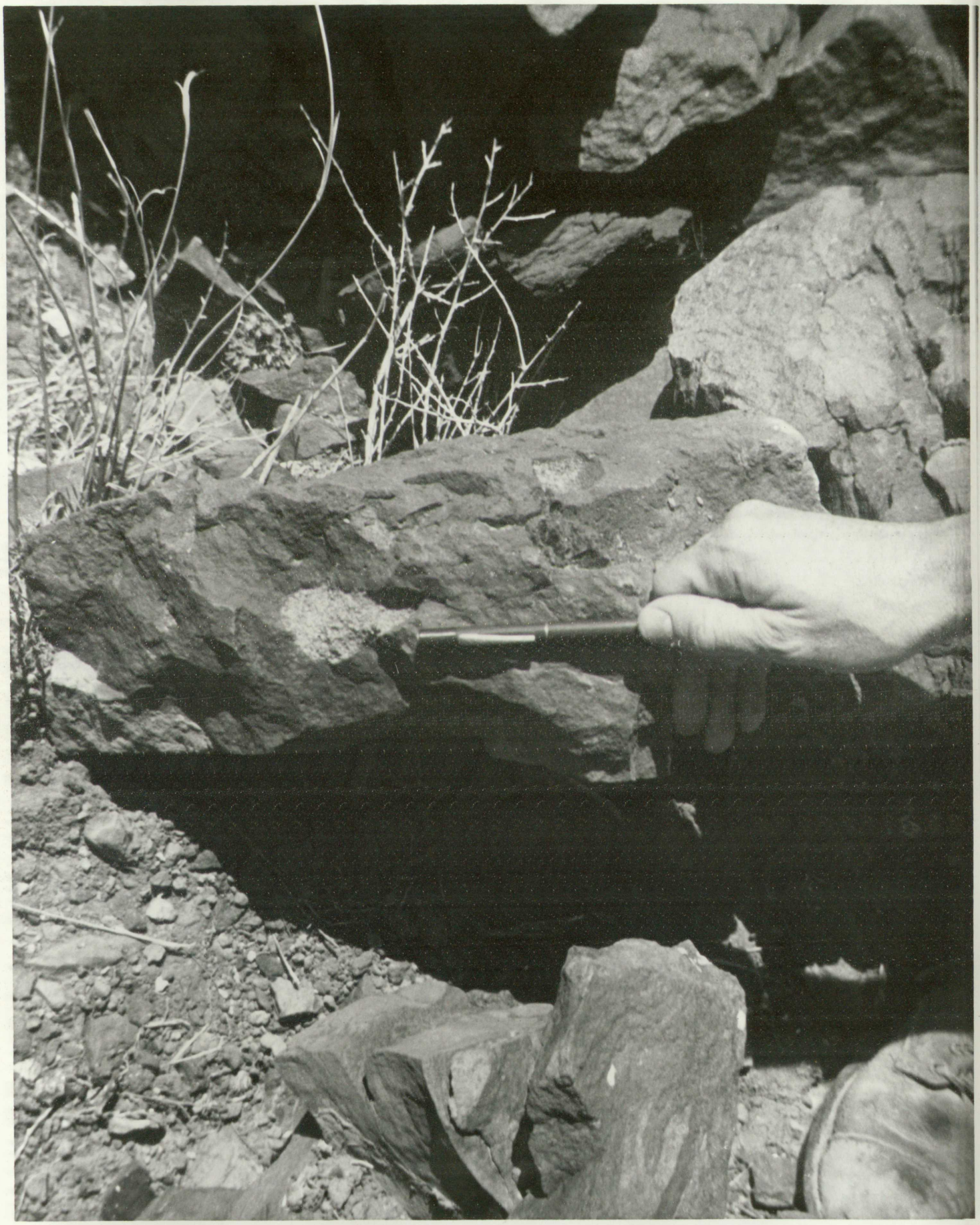

PLATE 11

Samples of Basalt and of Augite and Cumulars phäroliths

Figure 1. A piece of basalt from Plug 5. The area encircled and labeled D is a cumulars phärolith of olivine, diopside, and enstatite. (X $\frac{1}{2}$)

Figure 2. Six augite crystals weathered from the basalt. (X 2/5)

Figure 3. Augite phenocryst in basalt. (X $\frac{1}{2}$)

Figure 4. Augite phenocryst in basalt. (X $\frac{1}{2}$)

PLATE II

Samples of Basalt and of Augite and Cumularsphärolithe

Figure 1. A piece of basalt from Plug 5. The area encircled and labeled D is a cumularsphärolith of olivine, diopside, and enstatite. (X ½)

Figure 2. Six augite crystals weathered from the basalt. (X 2/5)

Figure 3. Augite phenocryst in basalt. (X ½)

Figure 4. Augite phenocryst in basalt. (X ½)

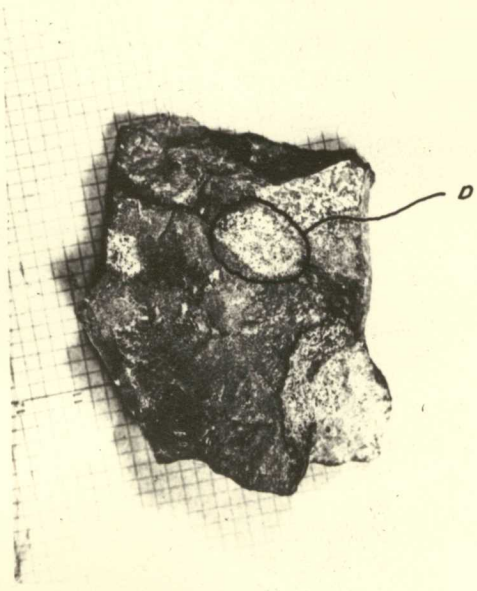

FIGURE 1

FIGURE 2

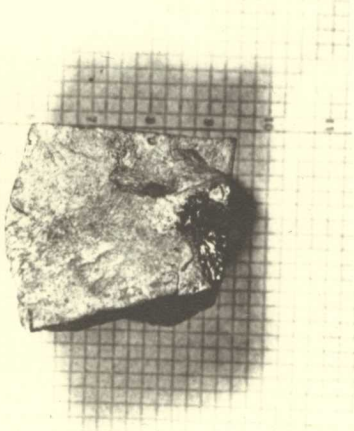

FIGURE 3

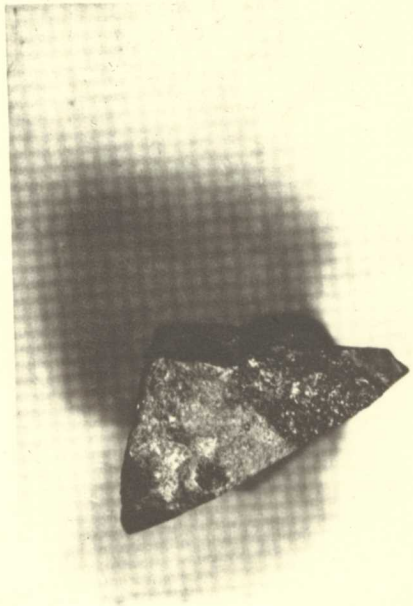

FIGURE 4

of augite microlites (Pl. 13, fig. 2). Some of the olivine has been altered to brown bastite or antigorite (Pl. 12, fig. 2). The bastite generally occurs in small circular concentric cryptocrystalline patches. The olivine comprises about 10 percent of the basalt.

Magnetite is the second most abundant mineral in the rock, comprising about 15 percent. It occurs as fine opaque powder throughout the groundmass and as a product of the reaction of the olivine and the pyroxenes with the basalt.

Quartz is common in the rock, either as almost completely absorbed grains with reaction rims of fine augite microlites (Pl. 14, fig. 1) or as partly absorbed grains (Pl. 13, figs. 1 and 3). Most of the quartz is probably derived from the sandstone plucked by the lava from the surrounding Mesaverde sandstone. Some quartz grains also occur in the granular masses of enstatite, diopside, and olivine (Pl. 13, fig. 4).

The diopside, enstatite, and spinel seem to be confined to cumularsphäroliths (Pl. 14, fig. 2) with or without olivine.

The augite occurs as large phenocrysts, ½ to 3 inches in diameter, or in granular masses with enstatite (Pl. 13, fig. 4). The large individual phenocrysts generally have a broad reaction rim. Pl. 11, fig. 3 and Pl. 12, figs. 3 and 4 show an augite phenocryst which is almost an inch in diameter and a reaction rim composed of magnetite near the

augite and glass with some magnetite and feldspar farther out. The augite in the granular masses is larger than the diopside or enstatite in similar masses (Pl. 13, fig. 4 and Pl. 14, fig. 2).

All the granular masses of diopside, enstatite, and/or olivine, and/or augite show reaction rims of glass with a concentration of magnetite.

Theoretical Considerations

The augite seems to be a product of the assimilation of quartz from sandstone by the basaltic magma.

A normal cooling over a long period of time would cause a basaltic magma to precipitate minerals according to Bowen's reaction series. The basalt would become more siliceous as the earliest formed minerals were removed from the magma by magmatic differentiation, that is, Bowen and others believe that, because the first minerals to precipitate from a basalt magma have a high specific gravity and are silica deficient, they will settle to the bottom of the fluid mass and leave the residual liquid with a relatively higher silica content. When the magma becomes siliceous it would tend to resorb any of the earlier formed minerals still present and to precipitate minerals farther down the reaction series.

Inasmuch as thin sections show the basalt in Plug 5 to be an olivine basalt, and the texture suggests rapid cooling, the magma probably did not have time to become

siliceous by differentiation--the olivine had probably just begun to crystallize. The resorption of the olivine and the subsequent formation of pyroxenes must have been caused by the assimilation of quartz and clay by the magma from the shaly sandstone of the Mesaverde formation.

An excess of silica plus olivine and part of the components of calcic feldspar would form diopside, enstatite, and spinel as follows:

$$FeO + CaO + Mg_2SiO_4 + Al_2O_3 + 2SiO_2 = MgSiO_3 + CaMgSi_2O_6 + FeAl_2O_4$$

The reaction:

$$MgSiO_3 + CaMgSi_2O_6 + FeAl_2O_4 = (Ca,Na)(Fe^{++},Mg,Fe^{+++})(Si,Al)Si_2O_6$$

would occur, under favorable magmatic conditions, transforming the spinel, diopside, and enstatite in a cumularsphärolith to augite, the excess Al_2O_3 and SiO_2 returning to the magma. The excess would then react with the olivine to form more augite to regain equilibrium.

The sandstone and shale inclusions in the basalt and the quartz grains indicate that the augite was formed at the expense of the olivine. The reaction lowered the temperature of the magma and, perhaps, along with normal cooling, helped chill the magma. The quick chilling stopped the reaction and prevented the resorption of all the olivine with the subsequent formation of augite.

PLATE 12

Photomicrographs of the Basalt

Figure 1. L is a labradorite phenocryst. The other large crystals are olivine. The groundmass is fine magnetite and labradorite microlites. (crossed nicols)(X 55)

Figure 2. A is bastite or antigorite. M is magnetite. (X 55)

Figure 3. The light area is a part of the large augite phenocryst shown in Plate 11, figure 3. It is surrounded by a narrow band of very fine magnetite which extends into fractures in the phenocryst. (X 55)

Figure 4. Figures 3 and 4 overlap. Outside the magnetite band there is a band of fine crystals and glass. This has been outlined in India ink. (X 55)

PLATE 12

Photomicrographs of the Basalt

Figure 1. L is a labradorite phenocryst. The other large crystals are olivine. The groundmass is fine magnetite and labradorite microlites. (crossed nicols)(X 55)

Figure 2. A is bastite or antigorite. M is magnetite. (X 55)

Figure 3. The light area is a part of the large augite phenocryst shown in Plate II, figure 3. It is surrounded by a narrow band of very fine magnetite which extends into fractures in the phenocryst. (X 55)

Figure 4. Figures 3 and 4 overlap. Outside the magnetite band there is a band of fine crystals and glass. This has been outlined in India ink. (X 55)

FIGURE 1

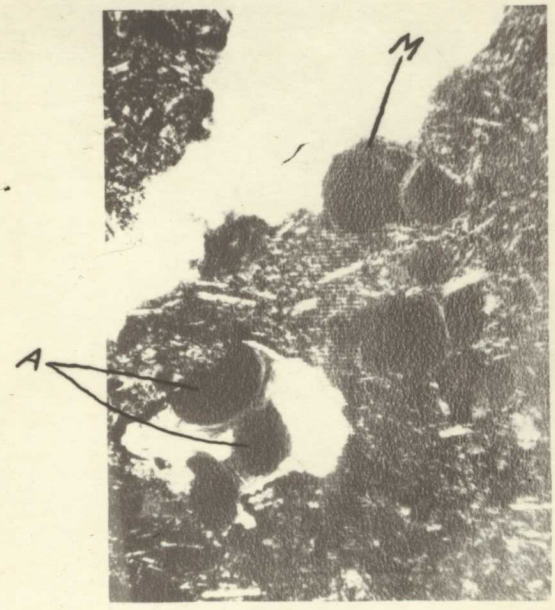

FIGURE 2

FIGURE 3

FIGURE 4

PLATE 13

Photomicrographs of the Basalt

Figure 1. A large quartz grain with a reaction rim of fine augite microlites. (X 55)

Figure 2. An olivine phenocryst with a similar reaction rim. (X 15)

Figure 3. A group of quartz grains that have been reacted upon by the basalt along the fractures. (crossed nicols)(X 15)

Figure 4. A is augite; E, enstatite; O, olivine; and Q, quartz. (crossed nicols)(X 15)

PLATE 13

Photomicrographs of the Basalt

Figure 1. A large quartz grain with a reaction rim of fine augite microlites. (X 55)

Figure 2. An olivine phenocryst with a similar reaction rim. (X 15)

Figure 3. A group of quartz grains that have been reacted upon by the basalt along the fractures. (crossed nicols)(X 15)

Figure 4. A is augite; E, enstatite; O, olivine; and Q, quartz. (crossed nicols)(X 15)

FIGURE 1

FIGURE 2

FIGURE 3

FIGURE 4

PLATE 14

Photomicrographs of the Basalt

Figure 1. An almost completely assimilated quartz grain. The reaction rim is principally augite and magnetite microlites. (X 15)

Figure 2. D is diopside; E, enstatite; and O, olivine. The black areas are spinel. (crossed nicols) (X 15)

PLATE 14

Photomicrographs of the Basalt

Figure 1. An almost completely assimilated quartz grain. The reaction rim is principally augite and magnetite microlites. (X 15)

Figure 2. D is diopside; E, enstatite; and O, olivine. The black areas are spinel. (crossed nicols) (X 15)

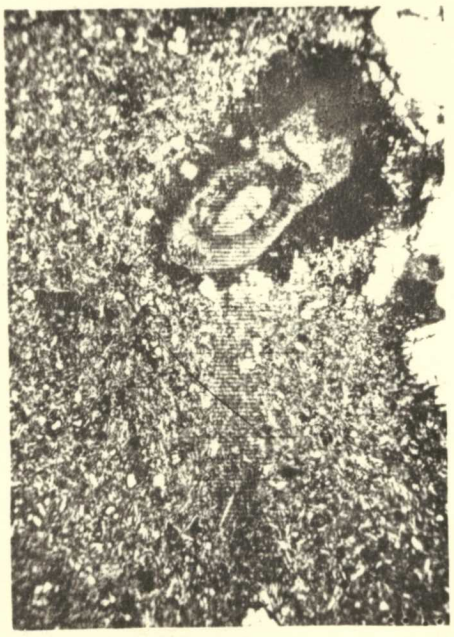

FIGURE 1

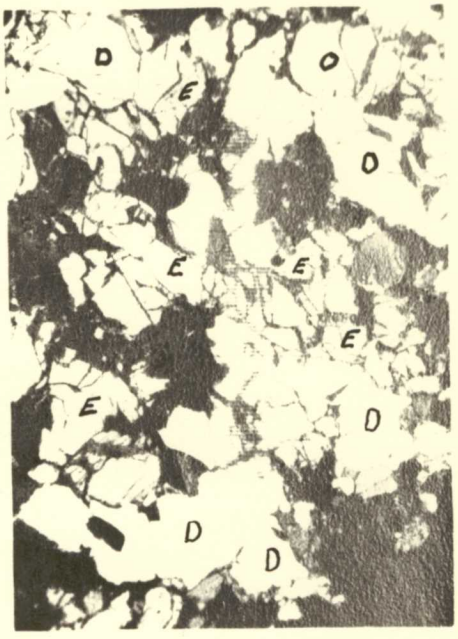

FIGURE 2

American Society for Testing Materials (1950), Alphabetical and Grouped Mineral Index of X-ray Diffraction Data.

Bunn, C. W. (1946), Chemical Crystallography, Clarendon Press, Oxford, 422 pages.

Buerger, M. J. (1942), X-ray Crystallography, John Wiley & Sons, Inc., 531 pages.

Donnay, G., and Donnay, J. D. H. (1951), Crystal Adjustment by Means of One Doubly Exposed X-ray Photograph, Pre-print, 5 pages.

Hunt, C. B. (1937), Igneous Geology and Structure of the Mount Taylor Volcanic Field, New Mexico, U. S. G. S. Professional Paper 189-B, 80 pages.

Internationale Tabellen Zur Bestimmung von Kristallstrukturen (1944), Vol. 1, page 102.

Johannsen, A. (1939), Petrography of Igneous Rocks, University of Chicago Press, Vol. 1, pages 172 and 207.

Johnson, D. W. (1907), Volcanic Necks of the Mt. Taylor Region, New Mexico, Geol. Soc. America Bull., Vol. 18, pages 303-324.

Shand, S. J. (1947), Eruptive Rocks, John Wiley & Sons, Inc., pages 69-87.

Turner, F. J., and Verhoogen, J. (1951), Igneous and Metamorphic Petrology, McGraw-Hill Book Co., Inc., pages 116-119.

Wahlstrom, E. E. (1950), Introduction to Igneous Petrology, John Wiley & Sons, Inc., 365 pages.

Warren, B. E., and Biscoe, J. (1931), Zeit. Krist. Vol. 80, page 391.

Winchell, A. N., and Winchell, H. (1951), Elements of Optical Mineralogy, Part 2, John Wiley & Sons, Inc., pages 411-418.


DIETER
BINDS
BETTER
DENVER, COLO.